Evaluation of Satellite-based Upper-troposphere Cloud-top Height Retrievals in Multilayer Cloud Conditions During TC4

Fu-Lung Chang[1], Patrick Minnis[2], J. Kirk Ayers[1], Matthew J. McGill[3], Rabindra Palikonda[1], Douglas A. Spangenberg[1], William L. Smith, Jr.[2], Christopher R. Yost[1]

(1) Science Systems and Applications, Inc., Hampton, Virginia
(2) NASA Langley Research Center, Hampton, Virginia
(3) NASA Goddard Space Flight Center, Greenbelt, Maryland

For submission to J. Geophys. Res. Special Issue on TC4

Corresponding author address:
Dr. Fu-Lung Chang
Mail Stop 420, NASA Langley Research Center, Hampton, Virginia 23681
Email: f.chang@larc.nasa.gov

Abstract

Upper-troposphere cloud-top heights (CTHs), restricted to cloud-top pressures (CTPs) < 500 hPa, inferred using four satellite retrieval methods applied to Twelfth Geostationary Operational Environmental Satellite (GOES-12) data are evaluated using measurements during the July-August 2007 Tropical Composition, Cloud and Climate Coupling Experiment (TC4). The four methods are the single-layer CO_2-absorption technique (SCO2AT), a modified CO_2-absorption technique (MCO2AT) developed for improving both single- and multi-layered cloud retrievals, a standard version of the Visible Infrared Solar-infrared Split-window Technique (old VISST), and a new version of VISST (new VISST) recently developed to improve cloud property retrievals. They are evaluated by comparing with ER-2 aircraft-based Cloud Physics Lidar (CPL) data taken during 9 days having extensive upper-troposphere cirrus, anvil and convective clouds. Compared to the 89% coverage by upper-tropospheric clouds detected by the CPL, the SCO2AT, MCO2AT, old VISST, and new VISST retrieved CTPs < 500 hPa in 76, 76, 69, and 74% of the matched pixels, respectively. Most of the differences are due to sub-visible and optically-thin cirrus clouds occurring near the tropopause that were detected only by the CPL. The mean upper-tropospheric CTHs for the 9 days are 14.2 (±2.1) km from the CPL and 10.7 (±2.1), 12.1 (±1.6), 9.7 (±2.9) and 11.4 (±2.8) km from the SCO2AT, MCO2AT, old VISST and new VISST, respectively. Compared to the CPL, the MCO2AT CTHs had the smallest mean biases for semitransparent high clouds in both single- and multi-layered situations whereas the new VISST CTHs had the smallest mean biases when upper clouds were opaque and optically thick. The biases for all techniques increased with increasing numbers of cloud layers. The transparency of the upper-layer clouds tends to increase with the numbers of cloud layers.

1. Introduction

Passive satellite instruments have long been used for monitoring large-scale cloud systems in time and space. Yet, the retrieved cloud properties are still subject to large uncertainties. Retrievals of cloud-top height (CTH), a fundamental cloud property, are often biased by 1.5 km or more, even for single-layered cloud systems [e.g., *Smith et al.*, 2008; *Menzel et al.*, 2008]. On average, those errors can exceed 3 km for thin upper-tropospheric cirrus clouds that are semitransparent in the infrared wavelengths [e.g., *Holz et al.*, 2008; *Chang et al.*, 2010]. In the presence of multilayer clouds, errors in the retrieved CTHs are often greater due to the assumption of a single-layered cloud employed in operational satellite retrieval techniques [*Chang et al.*, 2005, 2010; *Naud et al.*, 2005]. That is, the retrieval methods interpret the spectral radiances from a given scene as being the result of interactions among the radiances leaving the surface and scattering, absorption, and emission by the atmosphere and a cloud at one particular altitude. When a thin, high cloud overlaps a low cloud, the retrieved CTH is typically found somewhere between the two clouds, its value depending mainly on the high-cloud optical depth and the separation of the two cloud layers. To provide more accurate cloud observations for climate monitoring and the development and validation of cloud process models in weather forecasting, it is necessary to employ a different approach to determine CTH. Active sensors, i.e., cloud lidars and radars, at the surface [e.g., *Clothiaux et al.*, 2000], on aircraft [e.g., *McGill et al.*, 2004], and on satellites [*Winker et al.*, 2007; *Stephens and Kummerow*, 2007] are ideal for accurately determining the vertical layering of clouds, but are quite limited temporally or spatially. Until the challenges of actively sensing clouds on large spatial and relatively high-resolution temporal scales are overcome, it is necessary to develop and test new techniques for unscrambling the passively sensed radiances to retrieve more accurate cloud properties for both single- and multi-layer clouds.

Chang et al. [2010] recently developed a modified CO_2-absorption technique (MCO2AT) that uses two spectral channels, centered near 11 and 13.3 µm, to infer the CTH for the highest cloud whether for single- or multi-layered conditions. It differs from the traditional CO_2-slicing methods [e.g., *Smith and Platt*, 1978, *Wielicki and Coakley*, 1981; *Wylie and Menzel*, 1999; *Holz et al.*, 2008; *Menzel et al.*, 2008] in that it solves for the cloud-top radiating temperature using estimates for the effective background radiances, instead of using the clear-sky background radiances for the solution. Because the new approach utilizes the 11- and 13.3-µm channels on several newer operational geostationary satellites, such as the Twelfth Geostationary Operational Environmental Satellite Imager (GOES-12) [*Schmit et al.*, 2001], it has the potential for improving the inference of the upper-troposphere transmissive cloud properties in both single-layer and multilayer situations at relatively high temporal and spatial resolutions.

Cloud-top properties such as cloud effective radiating temperature, optical depth, and effective ice-crystal diameter are retrieved from geostationary satellite imager data in near-real time [*Minnis et al.*, 2008a] based on the Visible Infrared Solar-infrared Split-window Technique (hereafter referred as the old VISST) [*Minnis et al.*, 2010a]. The VISST is an operational algorithm developed at NASA Langley Research Center (LaRC) for retrieving satellite cloud optical and microphysical properties for the Cloud and the Earth's Radiant Energy System (CERES) and operational geostationary satellite projects. Since then, the old VISST has been modified to develop a new VISST algorithm [*Minnis et al.*, 2010b] for improving the GOES-12 retrievals of upper-tropospheric cloud optical and microphysical properties using model reflectances based on rough ice crystals [*Yang et al.*, 2008a,b], improved ozone and Rayleigh scattering corrections, and a new thick-cloud top height correction. In essence, the VISST, uses the cloud optical depth retrieved using the visible-wavelength reflectance to estimate the cloud emissivity based on the single-layer cloud assumption. Cloud-top effective temperature T_{eff} is then retrieved from the 10.8-μm radiance data by correcting for transmission through the cloud. An effective cloud height Z_{eff} corresponding to T_{eff} is inferred, which is usually located somewhere within the cloud, lower than the physical cloud top. Empirical methods are used to estimate the cloud physical top height CTH from T_{eff}. While the new VISST differs from the old version in many respects, the differences between the old and new VISST retrievals have not yet been evaluated.

Data taken during the NASA-sponsored Tropical Composition, Cloud, and Climate Coupling (TC4) Experiment conducted from Costa Rica during July and August 2007 [*Toon et al.*, 2010] are ideal for evaluating passive CTH retrievals from geostationary satellite data. The Cloud Physics Lidar (CPL) on the NASA ER-2 high-altitude aircraft made highly accurate CTH measurements during all of the TC4 flight hours. The flights were conducted during daylight and sampled the clouds at several local times, thus providing data at most solar zenith angles and at different points in the diurnal cycle of convection.

To date, the MCO2AT has only been tested against active sensor retrievals over limited mid-latitude regions. *Chang et al.*, [2010] found that the MCO2AT-inferred CTHs are significantly improved over the CTHs inferred by the single-layered CO_2-absorption technique (SCO2AT). Much additional testing of the MCO2AT and SCO2AT is needed to ensure that it works well in all conditions, including the high-altitude deep convective conditions in the tropics. The improvements in the VISST have not been quantified for any conditions. Since both the old and new VISSTs were used to analyze the same GOES-12 data during TC4 [*Minnis et al.*, 2010b], it is possible to determine how accurately the new VISST retrieves ice cloud top heights compared to the old VISST and the CO_2-absorption techniques (CO2ATs) using independent measurements from that experiment.

The primary objective of this paper is to evaluate the upper-troposphere CTHs (< 500 hPa) inferred by the MCO2AT and by the new VISST relative to the SCO2AT and old VISST, respectively. The TC4 CPL CTH data serve as the ground truth for all of the retrievals. This study focuses on the upper-troposphere clouds comprised of convective towers, optically-thick, optically-thin anvils and cirrus, as well as many multilayered clouds.

The paper is organized as follows. Section 2 describes the GOES-12 imager and the ER-2 CPL data used in this study. Section 3 describes the different methodologies of the SCO2AT, MCO2AT and the old and new VISST. Section 4 compares the GOES-12 CTH retrievals from the four techniques, which are evaluated by comparing with the aircraft CPL CTH data obtained during TC4. Analyses and discussions are also provided for optical-thin, optical-thick, and multilayer cloud scenarios. The final section gives the summary and conclusions.

2. Data

2.1 GOES-12 data

The GOES-12 imager at 0°N, 75°W was used to aid mission planning during TC4 and provide high temporal-resolution cloud products for the entire TC4 experimental area [*Minnis et al.*, 2010b; *Toon et al.*, 2010]. The GOES-12 imager 10.8- and 13.3-µm channels are used in the SCO2AT and MCO2AT for retrieving upper-troposphere cloud-top pressure

(CTP) as presented in Section 3.1. The 0.65-, 3.9-, 10.8- and 13.3-μm channel data are used by both the old and new VISST [*Minnis et al.*, 2010b] for retrieving the cloud effective temperature and cloud-top temperature (CTT) for clouds located at all altitudes as described in Section 3.2. The CTPs from the SCO2AT and MCO2AT and the CTTs from the two VISST algorithms are converted to CTHs using profiles of atmospheric pressure, temperature and height obtained from the National Centers for Environmental Prediction (NCEP) Global Forecast System (GFS) dataset [*Kalnay et al.*, 1990; *Kanamitsu et al.*, 1991].

Half-hourly observations taken by GOES-12 approximately 15 and 45 minutes after the UTC hours were analyzed during TC4. The half-hourly GOES-12 imagery and the old and new VISST cloud products were taken from the NASA Langley TC4 imagery and cloud product archives [*Minnis et al.*, 2010a; see http://www-angler.larc.nasa.gov/]. Those data have a nominal 4 km × 3.2 km spatial resolution at nadir. The original scanning resolution is about 4 km × 2.3 km (north-south direction × east-west direction) for the 10.8-μm channel and about 8 km × 2.3 km (north-south × east-west) for the 13.3-μm channel.

2.2 CPL data

The NASA ER-2 flew at an altitude of 20 km, well above the highest cloud tops. The CPL is an active lidar used on high-altitude aircraft to measure attenuated backscatter lidar signals at 355-, 532- and 1064-nm wavelengths and is highly sensitive to optically thin cirrus and sub-visible clouds [*McGill et al.*, 2002]. Cloud and aerosol backscatter and optical properties are retrieved from the CPL data at 1 s (~200 m along track) horizontal resolution and 30-m vertical resolution. The CPL retrievals provide the top and bottom heights of all layers detected by the lidar up to a maximum of 10 layers with cumulative optical depths up to ~3. To determine whether the CPL-detected upper-tropospheric cloud is above the 500-

hPa pressure level, the CPL uppermost CTHs are also converted to corresponding CTPs using the NCEP GFS profiles.

3. Techniques

3.1 CO2ATs

Two CO2ATs, i.e., SCO2AT and MCO2AT, are applied by following the methods described in *Chang et al.* [2010]. Note that methods of CO2ATs differ from the method of traditional CO_2-slicing techniques. The CO_2-slicing technique often uses several CO_2-absorption channels located in 13.3-14.3-μm wavelength range and requires at least two CO_2-absorption channels having different central wavelengths that are close enough so that the two spectral cloud emissivities can be assumed to be equal. The CO2ATs use only the radiance pair from the 10.8-μm window and the 13.3-μm CO_2-absorption channel to infer upper-troposphere CTH. The CO2ATs are based on the well-mixed nature of CO_2 gas in the upper troposphere. The difference between the 10.8- and 13.3-μm upwelling radiances due to the presence of an upper-troposphere cloud is thus used to infer the cloud-top pressure (CTP). However, CO2ATs are only useful for retrieving upper-troposphere clouds because the 13.3-μm radiance loses its sensitivity to low clouds, owing to an increased CO_2-absorption path length between the top of atmosphere (TOA) and the low cloud top. In this study, evaluations of the CO2ATs are conservatively restricted to only the CTHs retrieved above the 500-hPa level (~5.7 km in altitude) to maximize the signal-to-noise ratio and to avoid the effects of variable CO_2-gas concentrations in the lower troposphere.

The SCO2AT is briefly described first, followed by details of the MCO2AT. The SCO2AT applied to the GOES-12 imager data is similar to the radiance ratio methods described earlier by *McCleese and Wilson* [1976], *Smith and Platt* [1978] and *Wielicki and Coakley* [1981]. For simplicity, let us use the superscript 11 for the 10.8-μm channel and superscript 13 for the 13.3-μm channel.

By assuming cloud reflectance to be negligible at both the 10.8- and 13.3-μm channels, the satellite-observed radiances R_{obs}^{11} and R_{obs}^{13} for the two channels can thus be written as

$$R_{obs}^{11} = \varepsilon_c^{11} R_{ovc}^{11} + (1 - \varepsilon_c^{11}) R_{clr}^{11} \tag{1}$$

$$R_{obs}^{13} = \varepsilon_c^{13} R_{ovc}^{13} + (1 - \varepsilon_c^{13}) R_{clr}^{13} . \tag{2}$$

where $\varepsilon_c = e_c A_c$ denotes an effective cloud emissivity with e_c being the cloud emissivity and A_c being the cloud cover fraction of the imager pixel, R_{ovc} denotes the overcast radiance as $\varepsilon_c = 1$, and R_{clr} denotes the clear-sky radiance as $\varepsilon_c = 0$.

The clear-sky radiances R_{clr}^{11} and R_{clr}^{13} for specified surface temperature T_g and surface pressure P_g are given by

$$R_{clr}^{11}(T_g|P_g) = B^{11}(T_g)\xi^{11}(P_g) + \int_{P_g}^{0} B^{11}(T(P)) \frac{d\xi^{11}(P)}{d\ln P} d\ln P \tag{3}$$

$$R_{clr}^{13}(T_g|P_g) = B^{13}(T_g)\xi^{13}(P_g) + \int_{P_g}^{0} B^{13}(T(P)) \frac{d\xi^{13}(P)}{d\ln P} d\ln P , \tag{4}$$

where B^{11} and B^{13} denote the Planck functions and $\xi^{11}(P)$ and $\xi^{13}(P)$ denote the transmittances between the TOA (*P* = 0) and pressure-level *P* for the two associated channels. Similarly, the overcast radiances R_{ovc}^{11} and R_{ovc}^{13} for specific cloud-top temperature T_c and cloud-top pressure P_c are give by

$$R^{11}_{ovc}(T_c|P_c) = B^{11}(T_c)\xi^{11}(P_c) + \int_{P_c}^{0} B^{11}(T(P))\frac{d\xi^{11}(P)}{d\ln P}\,d\ln P \qquad (5)$$

$$R^{13}_{ovc}(T_c|P_c) = B^{13}(T_c)\xi^{13}(P_c) + \int_{P_c}^{0} B^{13}(T(P))\frac{d\xi^{13}(P)}{d\ln P}\,d\ln P\,. \qquad (6)$$

The computations in Eqs. (3)-(6) use the atmospheric profile data obtained from the NCEP GFS dataset [*Kalnay et al.*, 1990; *Kanamitsu et al.*, 1991] and the MODTRAN4 radiative transfer code [*Berk et al.*, 1999].

To solve for $T_c|P_c$ with specified $T_g|P_g$, the ratios of (1) and (2) are manipulated to yield

$$\frac{R^{13}_{obs} - R^{13}_{clr}(T_g|P_g)}{R^{11}_{obs} - R^{11}_{clr}(T_g|P_g)} = \frac{\varepsilon^{13}_{c}(R^{13}_{ovc}(T_c|P_c) - R^{13}_{clr}(T_g|P_g))}{\varepsilon^{11}_{c}(R^{11}_{ovc}(T_c|P_c) - R^{11}_{clr}(T_g|P_g))}\,. \qquad (7)$$

The solution of $T_c|P_c$ can thus be inferred by searching for the solutions of R^{11}_{ovc} and R^{13}_{ovc} that best satisfy (7) for the satellite-observed pair, R^{11}_{obs} and R^{13}_{obs}. The SCO2AT-inferred CTH is then derived by comparing the inferred $T_c|P_c$ to the atmosphere temperature/pressure and height profile data. Note that previous studies often assumed $\varepsilon^{11}_{c} \cong \varepsilon^{13}_{c}$ in Eq. (7). Here the relation between ε^{11}_{c} and ε^{13}_{c} is determined based on radiative transfer calculations [*Chang et al.*, 2010].

The MCO2AT is a modified version of the SCO2AT. As the SCO2AT assumes clouds are single-layered with a clear-sky background, the MCO2AT determines the effective background radiances R^{11}_{ebg} and R^{13}_{ebg} and their corresponding effective background temperature T_{ebg} and pressure P_{ebg} for the lower cloud in a multilayer cloud situation or for the clear-sky background for single-layer clouds. As such, Eq. (7) is modified in the MCO2AT by

$$\frac{R_{obs}^{13} - R_{ebg}^{13}(T_{ebg}|P_{ebg})}{R_{obs}^{11} - R_{ebg}^{11}(T_{ebg}|P_{ebg})} = \frac{\varepsilon_c^{13}(R_{ovc}^{13}(T_c|P_c) - R_{ebg}^{13}(T_{ebg}|P_{ebg}))}{\varepsilon_c^{11}(R_{ovc}^{11}(T_c|P_c) - R_{ebg}^{11}(T_{ebg}|P_{ebg}))}, \quad (8)$$

where

$$R_{ebg}^{11}(T_{ebg}|P_{ebg}) = B^{11}(T_{ebg})\xi^{11}(P_{ebg}) + \int_{P_{ebg}}^{0} B^{11}(T(P))\frac{d\xi^{11}(P)}{d\ln P}d\ln P \quad (9)$$

$$R_{ebg}^{13}(T_{ebg}|P_{ebg}) = B^{13}(T_{ebg})\xi^{13}(P_{ebg}) + \int_{P_{ebg}}^{0} B^{13}(T(P))\frac{d\xi^{13}(P)}{d\ln P}d\ln P. \quad (10)$$

To solve for $T_c|P_c$ using Eq. (8), the MCO2AT needs to determine $T_{ebg}|P_{ebg}$ using an iterative algorithm as illustrated in Figure 1. In the iterative algorithm, the solution of a SCO2AT-retrieved $T_c|P_c$ is first obtained using Eq. (7). If the SCO2AT $P_c < 500$ hPa, it proceeds to the MCO2AT iterative algorithm to estimate new $T_{ebg}|P_{ebg}$ and infer new $T_c|P_c$ using Eq. (8). Note that the inferred effective background radiance R_{ebg}^{11} is bound between the clear-sky radiance R_{clr}^{11} and the midway radiance ($R_{clr}^{11} + R_{obs}^{11}$)/2 whereas the inferred $T_c|P_c$ is bound by the tropopause [*Chang et al.*, 2010].

3.2 VISSTs

The VISST algorithm matches theoretically computed radiances with the GOES-12 imager-observed radiances at the 0.65-, 3.9-, 10.8-, and 13.3-μm channels to retrieve cloud parameters such as optical depth (OD), effective particle size, water phase, emissivity, effective cloud temperature, pressure and height, etc. The effective cloud temperature T_{eff} and OD are primarily retrieved from the 10.8- and 0.65-μm data. For retrieving properties of ice and water clouds, the hexagonal ice crystal and spherical water droplet models are assumed, respectively [*Minnis et al.*, 1998]. For semitransparent clouds, OD is small making the satellite-observed 10.8-µm brightness temperature larger than the physical temperature of cloud top. The value of T_{eff} is then corrected to account for the gray-body emission and transmission from below the cloud, using the cloud emissivity and transmissivity estimated from the retrieved OD [*Minnis et al.*, 1998, 2010a]. The retrieved T_{eff} is then converted to an effective cloud height Z_{eff} using the NCEP GFS atmospheric data.

The old VISST [*Minnis et al.*, 2010a] assumes that CTH is equivalent to Z_{eff} for clouds with OD > 6. For clouds with OD $\leq$ 6, empirical formulae are then applied to determine the CTHs for thin clouds. In the new VISST, several changes are made to improve the retrievals of OD and CTH. First, a cloud reflectance model based on the single-scattering properties of ice crystals having surface roughness [*Yang et al.*, 2008a,b] replaces the old ice-crystal model that was based on smooth-faced hexagonal columns. It was found that using the new rough-surfaced ice-crystal model often reduces the retrieved ice-cloud OD, but it can cause either an increase or decrease in OD, depending on the viewing and illumination angles. Second, a new ozone correction is applied to the visible channel retrieval because correction of the ozone absorption in the old version of VISST was too large. As detailed in *Minnis et al.* [2010a], the visible-channel ozone transmittance in the new VISST is reduced by ~12%. Additionally, the Rayleigh scattering optical depth was too large for GOES retrievals in the old VISST, so it was reduced in new VISST. Thus, the rough-surfaced ice-crystal model and the new ozone absorption and Rayleigh scattering corrections generally result in smaller retrieved ODs than their counterparts in the old VISST. For semitransparent clouds, the smaller ODs would result in the higher Z_{eff} in new VISST. The third correction for Z_{eff} derived in the new VISST is based on the study of *Minnis et al.* [2008b] to account for the differences between Z_{eff} and CTH. This correction is only applied for ice clouds with retrieved OD > 6, using an empirical model to adjust Z_{eff} towards CTH. Thus, most of the corrections should result in higher CTHs from the new VISST algorithm.

4. Results

4.1 Comparisons of Upper-troposphere CTHs

The CPL and GOES-12 matched data are analyzed from 9 selected ER-2 flight days during the July-August 2007 TC4 experiment. Data from four other days (July 14, 25, 29 and August 9) are not included here because they were taken during transit flights or flights dedicated to measuring boundary layer clouds and/or aerosols. The CPL uppermost CTHs were averaged every 10 s. The averaging time of 10 s implies a ground track of ~2 km since the ER-2 traveled at a speed of ~200 m/s. Each 10-s averaged CPL CTH was matched with collocated GOES-12 pixel data from the two closest imagery scan times, one scanned before and another scanned after the CPL time. Since the GOES-12 imager scans at 30-min intervals, the collocated GOES-12-retrieved CTHs from the two images scanned before and after were then linearly interpolated in time to match the CPL CTH observation. However, when only one image pixel had retrieved CTH, that pixel CTH was treated as a match to the CPL data if the observing time difference between the image pixel and CPL data was less than 3 minutes. It is noted that the different times and horizontal resolutions of the GOES-12 and CPL cloud data make the comparisons of CTHs from the two measurements somewhat problematic, for example, a cloud could appear or disappear between the 30-min intervals or it may only occur in part of the pixel. To reduce the impacts of cloud breaks and inhomogeneous CTHs, the comparisons between matched CPL and GOES-12 CTH data are restricted by two conditions: the 10-s CPL data detect 100% cloud coverage and the 10-s CPL averaged uppermost CTH is above the 500-hPa level.

Table 1 shows the numbers of matched data points obtained for the CPL and GOES-12 and those with CTHs above the 500-hPa level retrieved by the CPL, CO2ATs, and VISSTs from the nine flights. In each flight, the total numbers of matched data (N_{match}) are divided into three categories (under N_{CPL}), denoted by *h*, *m* and *l*, according to the statistics of each 10-s CP CTH data. The *h* category denotes for those satisfy aforementioned two conditions, i.e., the 10-s CPL had 100% cloud coverage and the 10-s mean uppermost CTH is above the 500-hPa level. The *m* category denotes those having a few CPL CTHs above the 500 hPa, but their 10-s mean CTH is below the 500-hPa level. The *l* category then denotes the remaining matched data points which had either lower CTHs or no cloud retrieved by the CPL. In the three categories, the number of matched data having a valid CTP < 500 hPa inferred by the CO2ATs, the old and new VISST are denoted in Table 1 by N_{CO2AT}, $N_{\mathrm{VISST\text{-}old}}$ and $N_{\mathrm{VISST\text{-}new}}$. Only those matched CPL and GOES-12 data in the *h* category are compared in this study. Numbers in the *m* and *l* categories may be less reliable and could indicate data mismatches or overestimations by individual satellite techniques.

In general, from comparisons of N_{match} and N_{CPL}, the CPL detected large percentages of CTP < 500 hPa (four days had ~100%). Based on N_{CO2AT}, the CO2ATs retrieved large percentages (75-98%) of those upper-troposphere clouds (CTP < 500 hPa), except for July 19 (~49%) and August 6 (~14%). The two versions of VISST also retrieved consistently large percentages of CTP < 500 hPa. The new VISST showed good agreement with the CO2ATs while the old VISST retrieved about 10% fewer than those from the new VISST. More than 2% of the matched data had some scattered CPL CTPs < 500 hPa within 10-s average CTPs that are greater than 500 hPa (the *m* category). Because of the inhomogeneous cloud top fluctuations and/or broken cloud fields for this category, large discrepancies between the CTP and GOES-12 retrieved CTPs are expected and are therefore excluded from the comparisons. About 9% of the matched data had no CPL < 500 hPa retrieved by CPL. Less than 0.2% of the pixels have no CTP < 500 hPa from the CPL, while CTPs < 500 hPa were retrieved by the CO2ATs and VISSTs (the *l* category).

Figure 2 illustrates the matched CTHs inferred by the new VISST (blue), old VISST (green), MCO2AT (red) and SCO2AT (purple) overlaid on the ER-2 CPL vertical cloud mask data for 4 flight days. Each figure shows a 3-hour period of matched data obtained during the ER-2 flights on August 8 (Fig. 2a), July 31 (Fig. 2b), July 17 (Fig. 2c) and July 19 (Fig. 2d), which were selected to demonstrate different cloud scenarios. An example shown in Figure 3 illustrates the GOES-12 imagery 0.65- (3a) and 10.8-μm (3b) data and the MCO2AT (3c) and new-VISST (3d) inferred CTPs for the data obtained at 14:45 UTC, August 8, 2007 for the TC4 region. The ER-2 aircraft trajectories (flying at 20-km altitude above the clouds) for the 3-hour time period shown in Figure 2a are also plotted in Figure 3. Note that the aircraft trajectory is for the flight time between 12:40:45 and 15:40:45 (UTC) whereas the GOES-12 images resemble the snapshot at 14:45 (UTC).

During August 8 (Fig. 2a), the ER-2 flew over several convective cores and anvils. Comparing the data from this flight (12:40:45-17:40:16) when the CO2ATs had valid CTH retrievals (CTP < 500 hPa), the CPL measured a mean (±standard deviations) CTH of 13.9 ±1.4 km whereas the MCO2AT, SCO2AT, new VISST, and old VISST inferred 12.3±1.1, 10.7±1.8, 11.4±2.5, and 9.7±2.4 km, respectively. Generally, good agreement among the CPL, MCO2AT, and new-VISST CTHs was found near the convective cores, but away from the cores their CTH differences increased as the anvil cloud optical depths decreased. The MCO2AT CTHs were sometimes a few kilometers lower and the new-VISST CTHs were sometimes much lower than the CPL heights. On average, when compared with the MCO2AT, the new-VISST CTHs were lower by 0.9 km, the old-VISST CTHs were lower by 2.6 km, and the SCO2AT CTHs were lower by 1.6 km.

On July 31 (Fig. 2b), the ER-2 flew over some geometrically thick anvils formed by a large mesoscale complex in the Pacific just off the coast of Costa Rica. The data from this flight (13:15:56-17:19:40) show that when the CO2ATs had valid CTH retrievals, the CPL measured a mean CTH of 16.3 ±0.3 km whereas the MCO2AT, SCO2AT, new VISST and old VISST inferred mean CTHs of 12.8±1.7, 12.2±2.0, 13.0±2.7, and 11.7±2.5 km, respectively. While all four techniques underestimated the optically thin anvil CTHs by more than 3 km, differences between their mean CTHs were generally quite small (within 1.3 km) with the new VISST being the highest and the old VISST being the lowest. It was also found that the new VISST had better agreement with the CPL for optically thicker anvils (cf. Fig. 2b) and convective cores (cf. Fig. 2a). This day also had the highest percentages of CTP < 500 hPa retrieved by all four techniques (CO2ATs ~98 %, new VISST ~95% and old VISST ~94%).

On July 17 (Fig. 2c), the ER-2 flew over a large mesoscale complex off the Pacific coast of Costa Rica. Many optically thin cirrus clouds were missed by the four techniques at the beginning of this flight. The CPL-measured CTHs showed large fluctuations over the mesoscale complex causing problems in collocating the CPL and GOES-12 imager data. The CPL detected CTP < 500 hPa ~94% of the time, compared to about 71, 66, and 60% for the CO2ATs, the new VISST and the old VISST, respectively. For the period 12:59:25-16:44:09

UTC, when CO2ATs retrieved CTP < 500 hPa, the associated mean CTHs were 12.8±1.8 km (CPL), 12.0±1.5 km (MCO2AT), 10.3±2.2 km (SCO2AT), 10.3±3.1 km (new VISST), and 8.8±3.0 km (old VISST).

On July 19 (Fig. 2d), the ER-2 flew over the cores of several convective systems in the Pacific and then over the Caribbean to measure Sahara dust and low-lying clouds. There were high-altitude sub-visible thin-cirrus clouds lying above the convective systems during the first couple of flight hours. The sub-visible, thin cirrus clouds were generally not well retrieved by the four satellite techniques, but the new VISST showed significant improvement in the CTH retrievals relative to the old VISST. Comparing the data when CO2ATs had valid CTP < 500 hPa, the mean CTHs inferred on this day were 14.5 ±1.3 km (CPL), 12.2 ±1.2 km (MCO2AT), 10.5 ±1.9 km (SCO2AT), 11.7 ±2.4 km (new VISST) and 9.2 ±3.0 km (old VISST). The later periods of this flight were mainly over low-lying stratocumulus clouds [*Toon et al.*, 2010]. Overall, the CPL detected ~59% of CTP < 500 hPa during the flight as compared to only ~29%, ~30% and ~25%, detected by the CO2ATs, new VISST, and old VISST, respectively.

On August 6 (Table 1), the CPL detected an extensive, thin layer of sub-visible high-altitude (~15 km) cirrus clouds that occurred high above a deck of low-altitude (~1 km) boundary-layer clouds [*Toon et al.*, 2010]. The sub-visible cirrus clouds were generally missed by the four satellite techniques, leading to the largest differences in Table 1 between N_{CPL} (1694), N_{CO2AT} (230), $N_{\mathrm{VISST\text{-}old}}$ (191) and $N_{\mathrm{VISST\text{-}new}}$ (242). The sub-visible cirrus clouds on this day are responsible for most of the undetected upper-troposphere clouds in the passive retrieval results.

Overall, there were a total of 15,028 matched data points as shown in Table 1. Out of these, ~89% or 13,387 pixels (N_{CPL}) had CPL-retrieved CTHs above 500 hPa. There were ~68% (N_{CO2AT}) having CO2AT-retrieved CTHs above 500 hPa (i.e., CTP < 500 hPa). The CO2ATs retrieved CTHs above 500 hPa only 0.5% of the time when the CPL did not retrieve a valid CTP < 500 hPa. The new VISST ($N_{VISST\text{-}new}$) retrieved CTPs < 500 hPa for ~66% of the pixels in contrast to 61% for the old VISST ($N_{VISST\text{-}old}$). The rates of overestimation by both new and old VISSTs are smaller than the 0.5% by the CO2ATs. Relatively speaking, when the CPL retrieved upper-tropospheric clouds (CTP < 500 hPa), the CO2ATs retrieved ~76%, the new VISST retrieved ~74% and the old VISST retrieved ~69% of such upper tropospheric clouds. The findings that large percentages (24-31%) of upper-tropospheric clouds were not retrieved by the satellite techniques are reasonable considering the large fractions of optically very thin cirrus clouds that occurred during the TC4 experiment [*Toon et al.*, 2010]. The lidar system is much more sensitive to optically thin clouds than the passive sensors on the GOES-12 imager, which results in more detection of high clouds by the CPL.

Figure 4 shows scatter plots comparing the CTHs retrieved from the four satellite techniques to those from the CPL for all 9 flight days when the CO2ATs retrieved CTPs < 500 hPa. The mean CTHs are 14.2±2.1, 10.7±2.1, 12.1±1.6, 9.7±2.9, and 11.4±2.8 km for the CPL, SCO2AT (4a), MCO2AT (4b), the old VISST (4c), and the new VISST (4d), respectively. The corresponding overall mean biases relative to the CPL are −3.5, −2.1, −4.5 km, and −2.8 km. The MCO2AT reduced the mean biases of the SCO2AT by 1.4 km whereas the new VISST reduced the mean biases of the old VISST by 1.7 km. Note that much better agreement between the new VISST and CPL are found for CTH > 14 km.

Unlike the new VISST, all of the SCO2AT (Figure 4a), MCO2AT (Figure 4b) and old VISST (Figure 4c) have generally underestimated the CTHs between 14-16.5 km.

4.2 Cloud Emissivities and Multilayer Clouds

Figure 5 shows the CTH differences (dz_c) between the CPL and the four passive methods as a function of the MCO2AT-inferred cloud 10.8-μm effective emissivity (ε_c^{11}). Results in the figure were obtained from the 9-day data shown in Figure 4. Overall mean biases, assuming that CPL CTHs were the truth, are −3.5±2.3 (SCO2AT), −2.1±2.0 (MCO2AT), −4.5±2.9 (old VISST), −2.8±2.8 (new VISST) km, as given in each sub-panel. For more opaque and likely optically thick clouds with $\varepsilon_c^{11} > 0.95$, the mean dz_c were found to be −1.9, −1.4, −2.4, and −0.2 km for the SCO2AT (Figure 5a), MCO2AT (Figure 5b), old VISST (Figure 5c), and new VISST (Figure 5d), respectively. The underestimation of CTH by 1.4-2.4 km for those nearly opaque clouds (except for the new VISST case) are consistent with earlier results found by *Sherwood et al.*, [2004], who showed that the satellite infrared-derived CTHs were 1-2 km below the physical cloud tops detected by lidar instruments. This underestimation appeared to have been largely corrected for optically thick clouds, using the method of *Minnis et al.*, [2008b] in the new-VISST algorithm (Figure 5d).

For less opaque clouds with $\varepsilon_c^{11} < 0.95$, the absolute differences increase progressively with decreasing ε_c^{11}. For instance, for semitransparent clouds at $\varepsilon_c^{11} \sim 0.3$, the mean dz_c were found to be −5.1 km (SCO2AT − CPL), −2.8 km (MCO2AT −CPL), −5.7 km (old VISST − CPL) and −3.9 km (new VISST − CPL). Note that the MCO2AT appeared to have more overestimated CTHs for less opaque clouds (ε_c^{11} < 0.8) and have the overall smallest mean dz_c compared to the SCO2AT (Fig. 5a) and two VISSTs (Figs. 5c and 5d).

To examine the impact of multilayer clouds on the retrievals, Figure 6 shows the CTH differences from Figure 5 plotted as a function of the 10-s averaged number of cloud layers (N_{layer}) retrieved by the CPL. In general, the absolute mean dz_c of all four techniques increase with increasing N_{layer}, except that the MCO2AT shows the smallest mean biases for all single- and multi-layered clouds and it systematically reduces the SCO2AT mean biases by ~40%. The increased dz_c with increasing N_{layer} as revealed in Figures 6a, 6c and 6d may be attributed to the single-layer cloud assumption used by the SCO2AT and the old and new VISSTs in multi-layered cases. It is also possible that the CPL retrieved more cloud layers when the uppermost or upper cloud layers were optically thinner in those cases. This may imply that the increase in N_{layer} is related to the decrease in ε_c^{11}.

Figures 7-9 present dz_c as a function of ε_c^{11} by separating the single-layered (Figure 7), two-layered (Figure 8), and multilayered (Figure 9) clouds. For the single-layered cases, the mean dz_c is fairly constant within each technique until ε_c^{11} falls below 0.5. For 0.5 < ε_c^{11} < 0.95, the MCO2AT has the smallest mean dz_c (–0.5 to −1.0 km) and it reduces the absolute mean biases of the SCO2AT by ~1 km from −1.88 (Fig. 7a) to -0.92 km (Fig. 7b). The new VISST also reduces the absolute mean biases of the old VISST significantly towards larger ε_c^{11}.

For the two-layered (Figure 8) and multilayered (Figure 9) cases, their mean differences behaved like those discussed in Figure 5 because the majority of TC4 clouds mainly consist of more than one cloud layer. Nonetheless, for two-layered and multilayered clouds, the absolute mean biases in all four techniques and in every bin of ε_c^{11} are generally twice as large as those from the single-layered conditions. The respective mean biases for SCO2AT, MCO2AT, old VISST, and new VISST are −1.88, −0.92, −2.52 and −0.84 km for single-layered cases (Figure 7), −3.27, −1.93, −4.12 and −2.47 km for two-layered (Figure 8), and −4.88, −3.03, −6.24 and −4.64 km for multilayered cases (Figure 9). Among the four techniques, the MCO2AT has the smallest absolute mean biases when $\varepsilon_c^{11} < 0.9$. Even though the MCO2AT was developed to account for multilayer cloud conditions, the mean biases of MCO2AT also increased significantly from −0.92 for single-layered to −3.03 for multilayered cases. This increase is likely caused by multiple transmissive upper-level layers. In those instances, the MCO2AT infers an average height for the multiple transmissive layers. Additionally, many of the upper-layer clouds in these cases are clouds that cannot be detected by the CO2AT even in single-layer conditions. Hence, there is not enough change in the radiances for the MCO2AT to account for the small optical depth of the uppermost cloud. Finally, it is worth noting that about 21% (89% – 68%) of the matched data had the CPL-retrieved CTP < 500 hPa, but had no CO2ATs CTP retrieval. Among these data, nearly half of them had VISST-retrieved CTHs and these are plotted in Figure 10a (old VISST) and Figure 10b (new VISST) as compared with the CPL CTHs. Since such cases were very optically thin clouds, it is not surprising to see that most of the VISST CTHs are much too low, especially since there were no MCO2AT/SCO2AT retrievals available. The mean CTHs in Figure 10 are 3.3 km for the old VISST and improved to 3.9 km for the new VISST as versus 13.2 km for the CPL. The ODs of these clouds were on the order of $\leq \sim 0.1$. The accuracy of their retrieved CTHs is, thus, limited by both the sensitivity and horizontal resolution of the passive satellite instruments like GOES-12.

5. Summary and Conclusions

Nine days of daytime upper-troposphere cloud-top height (CTH) measurements obtained from GOES-12 imager data and the ER-2 CPL data during the July-August 2007 TC4 were compared to evaluate four satellite retrieval techniques for processing enhanced satellite single-layer and multilayer cloud property retrieval products at NASA Langley Research Center (LaRC) [*Minnis et al.*, 2008, 2010a,b]. The comparisons focused on upper-tropospheric clouds retrieved with CTP < 500 hPa using a standard single-layered CO_2-absorption technique (SCO2AT), a modified CO_2-absorption technique (MCO2AT), an earlier version of a Visible-Infrared-Shortwave-Split-window Technique (old VISST), and a recently-improved version of the VISST (new VISST).

Among the four techniques, the MCO2AT generally produces better agreement with the CPL for optically thin clouds when CTPs < 500 hPa were retrieved. The MCO2AT also has the best performance for all upper-transmissive clouds that are in single- and multi-layered conditions. It yields mean CTHs that exceed the mean SCO2AT CTH by ~1 km and, thus, is 40% less biased than the SCO2AT. The new VISST produces more accurate CTHs for the tropical upper-tropospheric clouds compared to the old VISST. The new correction for adjusting cloud effective height Z_{eff} in the old VISST to CTH employed in the new VISST algorithm produced the best agreement with the CPL for optically thick clouds. The new ozone correction and new ice crystal models, also employed in the new VISST, increased the detection of upper-tropospheric transmissive clouds. Overall, the new VISST algorithm enhanced the cirrus cloud detection by more than 5% compared to the old VISST algorithm.

The overall correction in the new VISST CTHs yielded a nearly unbiased result for optically thick clouds.

The evaluations of the four satellite techniques are important because the old VISST and MCO2AT algorithms are currently operating together to provide satellite-retrieved cloud property products at LaRC for single- and multi-layered clouds. The new VISST algorithm is expected to improve those cloud products. In comparisons with the CPL CTHs, the mean CTH biases with the MCO2AT are smaller by a factor of ~1.7 than those with the SCO2AT whereas the mean biases for the new VISST are smaller by a factor of ~1.6 than those for the old VISST. Overall, the CPL retrieved ~89% of the data with CTPs < 500 hPa whereas the SCO2AT, MCO2AT, old VISST, and new VISST retrieved 76, 76, 69, and 74% of those, respectively. When both the CPL and CO2ATs retrieved CTPs < 500 hPa, the mean CTHs from the CPL, SCO2AT and MCO2AT are 14.2±2.1, 10.7±2.1, and 12.1±1.6 km and their associated mean CTHs from the old and new VISSTs are 9.7±2.9 and 11.4±2.8 km, respectively. These results are encouraging when one considers the large percentages of semi-transparent upper-tropospheric clouds found during TC4. Although the MCO2AT CTHs are generally in better agreement with the CPL data, a mean bias of −2.1 km in MCO2AT CTHs found here for the TC4 tropical clouds is twice as large as the mean bias of about −1 km shown in *Chang et al.* [2010] who evaluated the MCO2AT-inferred CTHs for midlatitude clouds between 20°N-55°N. The larger mean bias found here is likely owing to the high occurrences of very optically thin cirrus clouds during TC4. However, both studies show that the MCO2AT-inferred CTHs are on average ~1.4 km higher than the SCO2AT-inferred CTHs.

As demonstrated in this study, the main cause of the CTH biases in all four satellite techniques applied to the GOES-12 imager data is associated with the semi-transparencies of tropical upper-tropospheric clouds. Their retrieval biases increased progressively as the cloud effective emissivity decreased below about 0.5. Further analysis on multilayered clouds also showed that the mean CTH biases increased from single-layered cases to multilayered cases in all four techniques. However, larger uncertainties were still associated mainly with upper-transmissive clouds having emissivities less than ~0.5. It was found that the mean biases increased with increasing number of cloud layers because the multilayered clouds were associated with more upper-transmissive cloud layers..

From the perspective that the MCO2AT uses only the infrared data at 10.8- and 13.3-μm channels, the technique can be applied equally for daytime and nighttime observations and is applicable to the Spinning Enhanced Visible and Infrared Imager (SEVIRI) on *Meteosat*-8 and -9, the Moderate-resolution Imaging Spectroradiometer (MODIS) on *Terra* and *Aqua*, and the upcoming GOES-R imager series [*Schmit et al.*, 2005]. The new VISST algorithm can be further improved using the MCO2AT. Another application of the MCO2AT is for multilayer cloud retrieval as shown in *Chang and Li* [2005]. The MCO2AT in conjunction with the new VISST has recently been developed for an integrated multilayer cloud retrieval algorithm as illustrated in *Minnis et al.* [2010a]. Future work requires more validation studies for more assessment of the MCO2AT, the new VISST, and the multilayer retrieval technique.

Acknowledgements.

This research was supported by the NASA Radiation Science Program TC4 project, the NASA Applied Sciences Program, the Department of Energy Atmospheric Radiation Measurement Program through Interagency Agreement, DE-AI02-07ER64546, and the NOAA Center for Satellite Applications and Research GOES-R program.

References

Berk, A., et al. (1999), MODTRAN4 v. 2.0 User's Manual, Air Force Geophysics Laboratory Tech. Rep. AFGL-TR-89-0122, 98 pp., Air Force Mat. Comm., Hanscomb AFB, Mass.

Chang, F.-L., and Z. Li (2005), A new method for detection of cirrus overlapping water clouds and determination of their optical properties, *J. Atmos. Sci.*, *62*, 3993–4009.

Chang, F.-L., P. Minnis, B. Lin, M. M. Khaiyer, R. Palikonda, and D. A. Spangenberg (2010), A modified method for inferring upper-troposphere cloud-top height using the GOES-12 imager 10.7- and 13.3-µm data, *J. Geophys. Res.*, in press.

Clothiaux, E. E., T. P. Ackerman, G. G. Mace, K. P. Moran, R. T. Marchand, M. Miller, and B. E. Martner (2000), Objective determination of cloud heights and radar reflectivities using a combination of active remote sensors at the ARM CART Sites, *J. Appl. Meteorol.*, *39*, 645-665.

Holz, R. E., S. A. Ackerman, F. W. Nagle, R. Frey, S. Dutcher, R. E. Kuehn, M. A. Vaughan, and B. Baum (2008), Global Moderate Resolution Imaging Spectroradiometer (MODIS) cloud detection and height evaluation using CALIOP, *J. Geophys. Res.*, 113, D00A19, doi:10.1029/2008JD009837.

Kalnay, E., M. Kanamitsu, and W. E. Baker (1990), Global numerical weather prediction at the National Meteorological Center, *Bull. Am. Meteorol. Soc.*, *71*, 1410-1428.

Kanamitsu, M., and coauthors (1991), Recent changes implemented into the Global Forecast System at NMC, *Weather and Forecasting*, *6*, 425-435.

McCleese, D. J., and L. S. Wilson (1976), Cloud top heights from temperature sounding instruments, *Q. J. R. Meteorol. Soc.*, *102*, 781-790.

McGill, M. J., D. L. Hlavka, W. D. Hart, J. D. Spinhirne, V. S. Scott, and B. Schmid (2002), The Cloud Physics Lidar: Instrument description and initial measurement results, *Applied Optics*, *41*, 3,725-3,734.

McGill, M. J., L. Li, W. D. Hart, G. M. Heymsfield, D. L. Hlavka, P. E. Racette, L. Tian, M. A. Vaughan, and D. M. Winker (2004), Combined lidar-radar remote sensing: Initial results from CRYSTAL-FACE, *J. Geophys. Res.,* 109, doi: 10.1029/2003JD004030.

Menzel, W. P., and coauthors, (2008), MODIS global cloud-top pressure and amount estimation: Algorithm description and results , *J. Climate Appl. Meteorol.*, *47*, 1175-1198.

Minnis, P., D. P. Kratz, J. A. Coakley, Jr., M. D. King, D. Garber, P. Heck, S. Mayor, D. F. Young, and R. Arduini (1995), Cloud optical property retrieval (Subsystem 4.3), Clouds and the Earth's Radiant Energy System (CERES), Algorithm Theoretical Basis Document, 3, Cloud analyses and radiance inversions (Subsystem 4), NASA RP 1376, 3, edited by CERES Science Team, pp. 135-176.

Minnis, P., D. P. Garber, D. F. Young, R. F. Arduini, and Y. Takano (1998), Parameterization of reflectance and effective emittance for satellite remote sensing of cloud properties, *J. Atmos. Sci.*, *55*, 3313-3339.

Minnis, P., and Co-authors (2008a), Near-real time cloud retrievals from operational and research meteorological satellites, *Proc. SPIE Europe Remote Sens. 2008*, Cardiff, Wales, UK, 15-18 September, **7107-2**, 8 pp.

Minnis, P., C. R. Yost, S. Sun-Mack, and Y. Chen (2008b), Estimating the physical top altitude of optically thick ice clouds from thermal infrared satellite observations using CALIPSO data, *Geophys. Res. Lett.*, *35*, L12801, doi:10.1029/2008GL033947.

Minnis, P., and coauthors (2010a), CERES Edition-2 cloud property retrievals using TRMM VIRS and Terra and Aqua MODIS data, Part I: Algorithms, *IEEE Trans. Geosci. Remote Sens.*, submitted.

Minnis, P., and coauthors (2010b), Cloud properties determined from GOES and MODIS data during TC4, submitted to *J. Geophys. Res.*, this issue.

Naud, C., J. Muller, and P. de Valk (2005), On the use of ICESAT-GLAS measurements for MODIS and SEVIRI cloud-top height accuracy assessment. *Geophys. Res. Lett.*, 32, L19815, doi: 10.1029/2005GL023275.

Rossow, W. B., and R. A. Schiffer (1999), Advances in understanding clouds from ISCCP, *Bull. Am. Meteorol. Soc.*, *80*, 2261-2287.

Schmit, T. J., E. M. Prins, A. J. Schreiner, and J. J. Gurka (2001), Introducing the GOES-M imager, *National Weather Assoc. Digest*, *25*, 28-37.

Schmit, T. J., M. M. Gunshor, W. P. Menzel, J. J. Gurka, J. Li, and A. S. Bachmeier (2005), Introducing the next-generation Advanced Baseline Imager on GOES-R, *Bull. Am. Meteorol. Soc.*, *86*, 1079-1096.

Sherwood, S. C., J.-H. Chae, P. Minnis, and M. McGill (2004), Underestimation of deep convective cloud tops by thermal imagery, *Geophys. Res. Lett.*, *31*, 10.1029/2004GL019699.

Smith, W. L., and C. M. R. Platt (1978), Comparison of satellite-deduced cloud heights with indications from radiosonde and ground-based laser measurements, *J. Appl. Meteorol.*, *17*, 1796-1802.

Smith, W. L., Jr., P. Minnis, H. Finney, R. Palikonda, and M. M. Khaiyer (2008), An evaluation of operational GOES-derived single-layer cloud top heights with ARSCL over the ARM Southern Great Plains site, *Geophys. Res. Lett.*, *35*, L13820, doi:10.1029/2008GL034275.

Stephens, G. L., and C. D. Kummerow (2007), The Remote Sensing of Clouds and Precipitation from Space: A Review, *J. of Atmos. Sci.*, 64, 3742–3765.

Toon, O. B., and Co-authors (2010), Planning and implementation of the Tropical Composition, Cloud and Climate Coupling Experiment (TC4), *J. Geophys. Res.*, this issue.

Wielicki, B. A., and J. A. Coakley Jr. (1981), Cloud retrieval using infrared sounder data: Error analysis, *J. Appl. Meteorol.*, *20*, 157-169.

Winker, D. M., W. H. Hunt, and M. J. McGill (2007), Initial performance assessment of CALIOP, *Geophys. Res. Lett.*, 34, L19803, doi:10.1029/2007GL030135.

Wylie, D. P., and W. P. Menzel, (1999), Eight years of high cloud statistics using HIRS. *J. Climate*, *12*, 170–184.

Yang, P., G. W. Kattawar, G. Hong, P. Minnis, and Y. X. Hu (2008a), Uncertainties associated with the surface texture of ice particles in satellite-based retrieval of cirrus clouds: Part I. Single-scattering properties of ice crystals with surface roughness, *IEEE Trans. Geosci. Remote Sens.*, 46(7), 1940-1947.

Yang, P., G. W. Kattawar, G. Hong, P. Minnis, and Y. X. Hu (2008b), Uncertainties associated with the surface texture of ice particles in satellite-based retrieval of cirrus clouds: Part II. Effect of particle surface roughness on retrieved cloud optical thickness and effective particle size, *IEEE Trans. Geosci. Remote Sens.*, 46(7), 1948-1957.

Table 1 ER-2 flight dates, time periods, numbers of CPL and GOES-12 matched data points (N_{match}) and numbers of the data points having valid CTP < 500 hPa from the CPL (N_{CPL}), CO2ATs (N_{CO2AT}), old VISST ($N_{VISST\text{-}old}$) and new VISST ($N_{VISST\text{-}new}$). The numbers in parentheses under N_{CPL} indicate the CPL data having either partially (*m* category) or no ((*l* category) CTP < 500 hPa.

Date	Time	N_{match}	N_{CPL}	N_{CO2AT}	$N_{VISST\text{-}old}$	$N_{VISST\text{-}new}$
Jul. 17	12:59:25-16:44:09	1348	1262 *h*	963	806	890
			(39) *m*	6	4	6
			(47) *l*	1	1	1
Jul. 19	12:55:21-17:51:41	1777	1053 *h*	513	450	528
			(71) *m*	1	1	1
			(653) *l*	0	0	0
Jul. 22	12:29:23-17:15:45	1717	1628 *h*	1475	1259	1417
			(52) *m*	27	6	13
			(37) *l*	4	4	5
Jul. 24	12:11:31-18:14:42	2179	1745 *h*	1292	1225	1312
			(61) *m*	6	5	5
			(373) *l*	10	8	9
Jul. 31	13:15:56-17:19:40	1462	1462 *h*	1435	1379	1396
			(0) *m*	0	0	0
			(0) *l*	0	0	0
Aug. 3	13:49:16-17:51:17	1452	1452 *h*	1349	1113	1213
			(0) *m*	0	0	0
			(0) *l*	0	0	0
Aug. 5	13:21:29-16:58:11	1298	1298 *h*	1244	1143	1218
			(0) *m*	0	0	0
			(0) *l*	0	0	0
Aug. 6	12:40:47-18:14:03	1999	1694 *h*	230	191	242
			(84) *m*	1	3	1
			(221) *l*	0	0	0
Aug. 8	12:40:45-17:40:16	1796	1793 *h*	1724	1568	1667
			(2) *m*	1	0	1
			(1) *l*	0	0	0

Figure Captions

Fig. 1 Schematic diagram for illustrating the SCO2AT and MCO2AT algorithms.

Fig. 2 Comparisons of the different CTHs inferred from the GOES-12 imager data using the new-VISST (blue), old-VISST (green), SCO2AT (purple) and MCO2AT (red). The CPL cloud vertical mask is shown in grey. (a) for August 8 between 12:40:45-15:40:45 UTC. (b) for July 31 between 13:15:56-16:15:56 UTC. c) for July 17 between 12:59:25-15:59:25 UTC. d) for July 19 between 12:55:21-15:55:21 UTC.

Fig. 3 GOES-12 0.65-µm (a) and 10.8-µm (b) images and associated MCO2AT (c) and new-VISST (d) derived CTHs for 14:45 UTC 8 August 2007 over the TC4 area with overlaid ER-2 flight tracks between 12:40:45 and 13:40:45 (cyan), 13:40:45 and 14:40:45 (blue), and 14:40:45 and 15:40:45 (yellow).

Fig. 4 Comparisons of CTHs inferred from the GOES-12 imager and the CPL data. (a) for the SCO2AT vs CPL. (b) for the MCO2AT vs CPL. (c) for the old VISST vs CPL. (d) for the new VISST vs CPL.

Fig. 5 CTH difference dz_c as a function of the 10.8-µm cloud effective emissivity ε_c^{11}. (a) for SCO2AT minus CPL. (b) for MCO2AT minus CPL. (c) for old VISST minus CPL. (d) for new-VISST minus CPL. Thick-grey lines represent the running means.

Fig. 6 CTH difference dz_c as a function of the number of cloud layers N_{layer}. (a) for SCO2AT minus CPL. (b) for MCO2AT minus CPL. (c) for old VISST minus CPL. (d) for new VISST minus CPL. Thick-grey lines represent the running means.

Fig. 7 Same as in Fig. 5, except for the single-layered ($N_{layer} = 1$) clouds.

Fig. 8 Same as in Fig. 5, except for the two-layered ($1 < N_{layer} \leq 2$) clouds.

Fig. 9 Same as in Fig. 5, except for the multilayered ($N_{layer} > 2$) clouds.

Fig. 10 Comparisons of the old-VISST (a) and new-VISST (b) CTHs with the CPL CTH when there was no SCO2AT/MCO2AT retrieval.

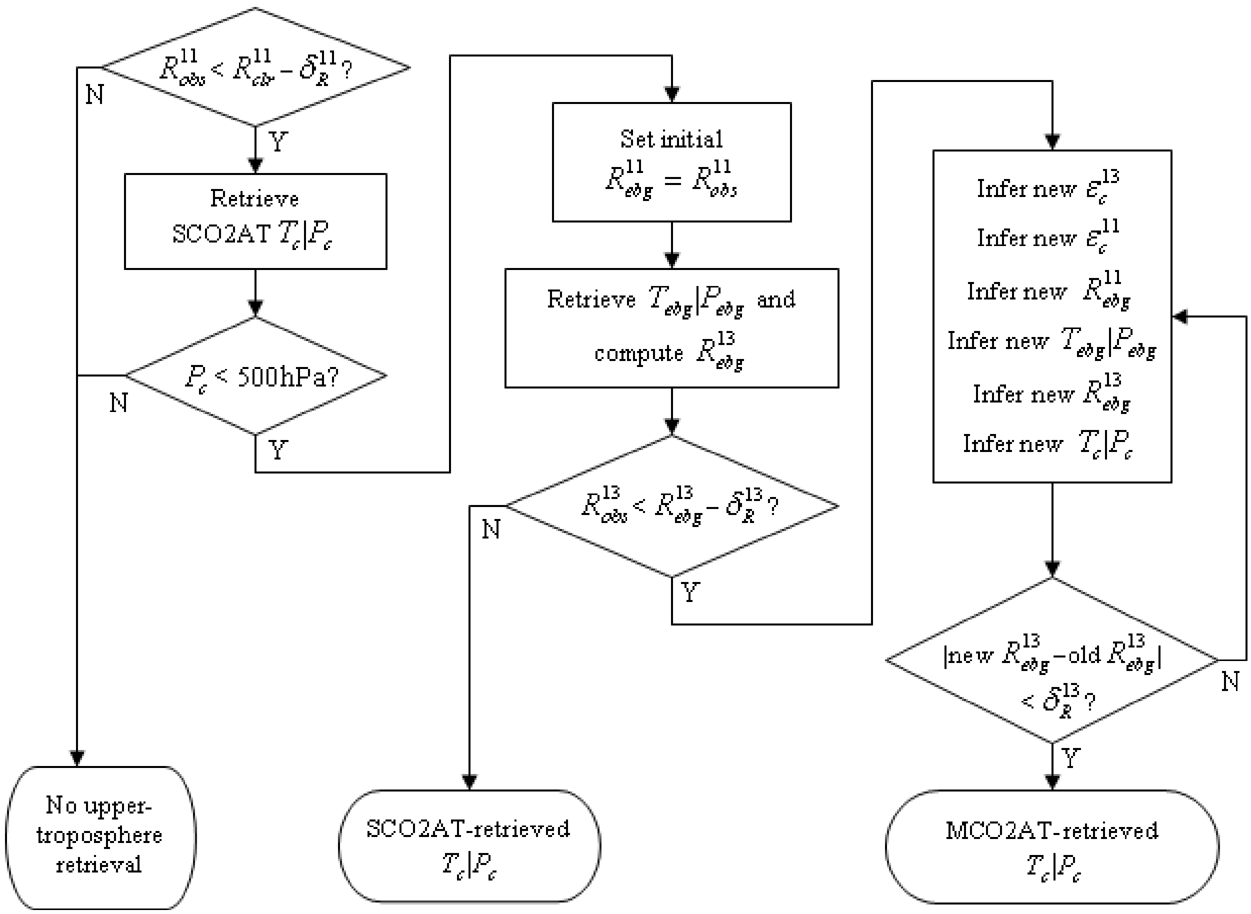

Fig. 1 Schematic diagram for illustrating the SCO2AT and MCO2AT algorithms.

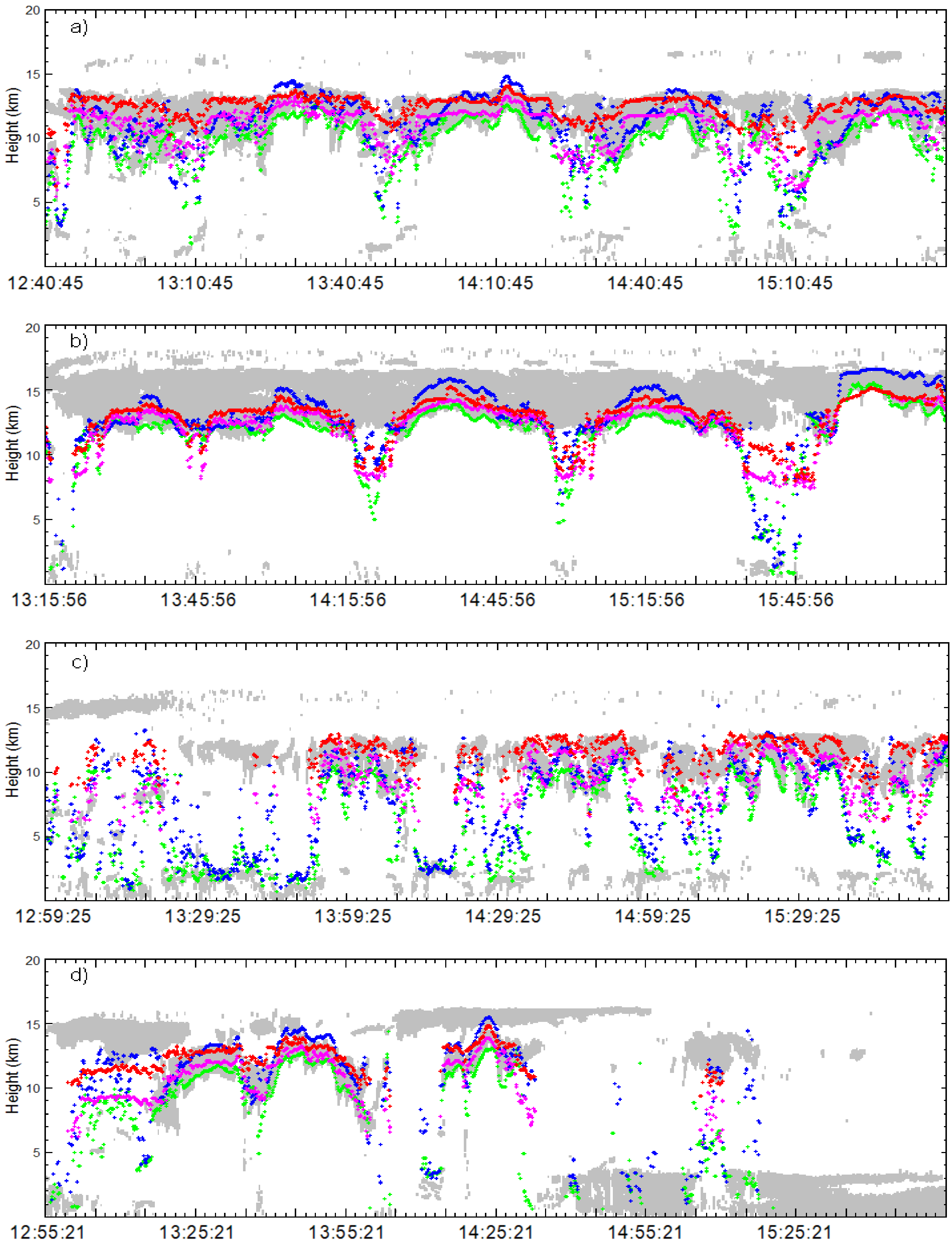

a)
b)
c)
d)
Height (km)
20
15
10
5
12:40:45
13:10:45
13:40:45
14:10:45
14:40:45
15:10:45
13:15:56
13:45:56
14:15:56
14:45:56
15:15:56
15:45:56
12:59:25
13:29:25
13:59:25
14:29:25
14:59:25
15:29:25
12:55:21
13:25:21
13:55:21
14:25:21
14:55:21
15:25:21

Fig. 2 Comparisons of the different CTHs inferred from the GOES-12 imager data using the new-VISST (blue), old-VISST (green), SCO2AT (purple) and MCO2AT (red). The CPL cloud vertical mask is shown in grey. (a) for August 8 between 12:40:45-15:40:45 UTC. (b) for July 31 between 13:15:56-16:15:56 UTC. c) for July 17 between 12:59:25-15:59:25 UTC. d) for July 19 between 12:55:21-15:55:21 UTC.

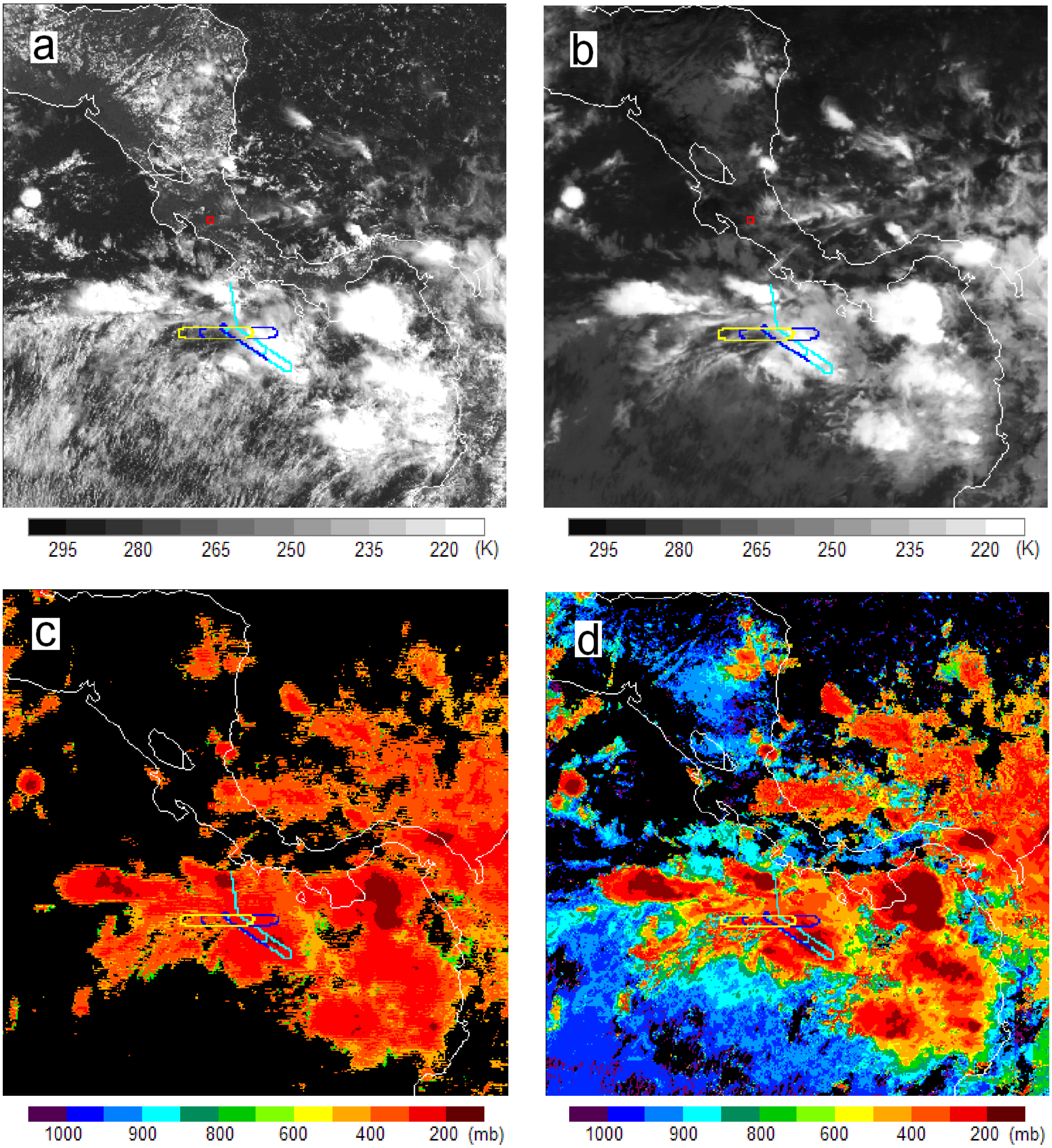

Fig. 3 GOES-12 0.65-µm (a) and 10.8-µm (b) images and associated MCO2AT (c) and new-VISST (d) derived CTHs for 14:45 UTC 8 August 2007 over the TC4 area with overlaid ER-2 flight tracks between 12:40:45 and 13:40:45 (cyan), 13:40:45 and 14:40:45 (blue), and 14:40:45 and 15:40:45 (yellow).

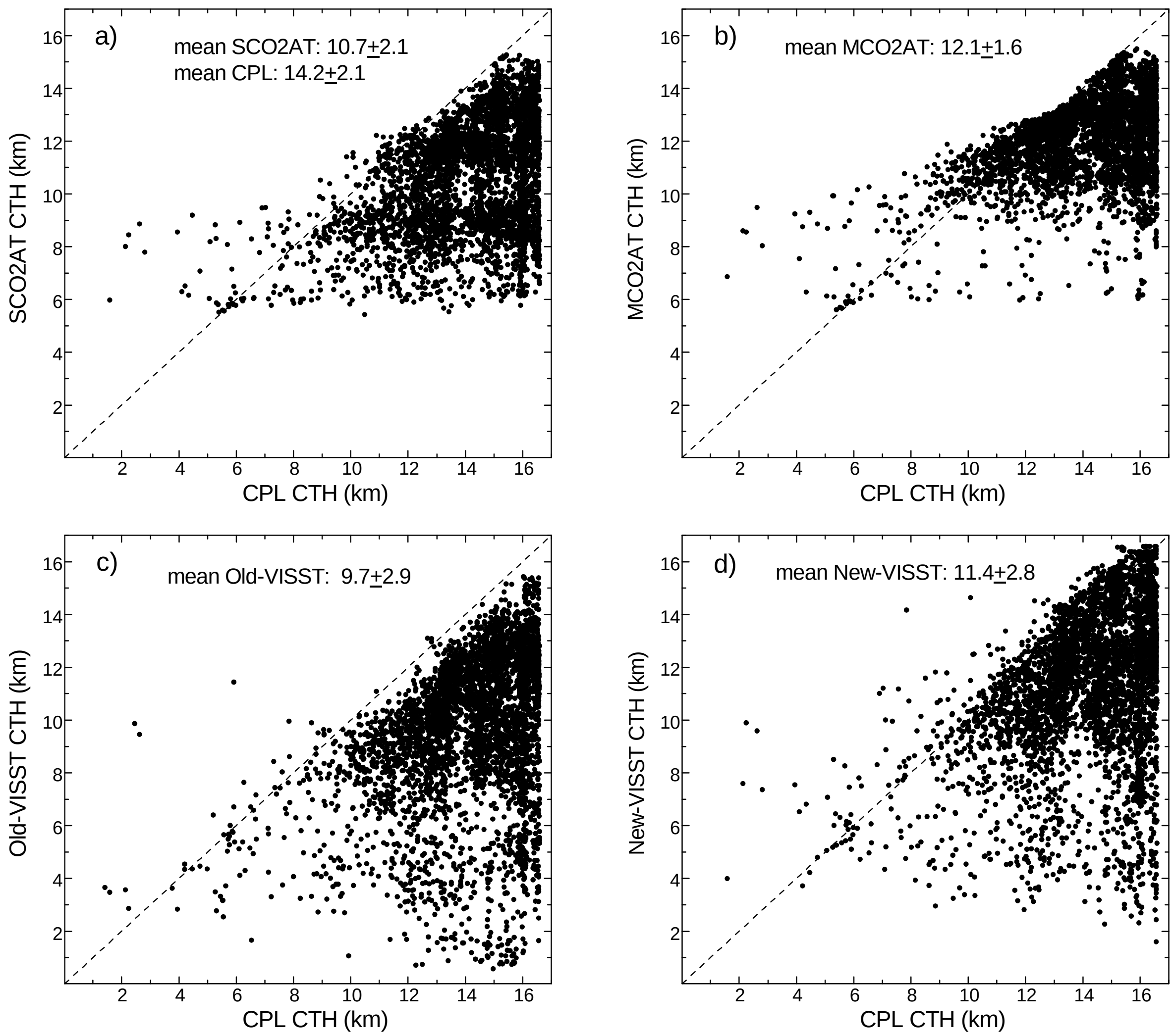

Fig. 4 Comparisons of CTHs inferred from the GOES-12 imager and the CPL data. (a) for the SCO2AT vs CPL. (b) for the MCO2AT vs CPL. (c) for the old VISST vs CPL. (d) for the new VISST vs CPL.

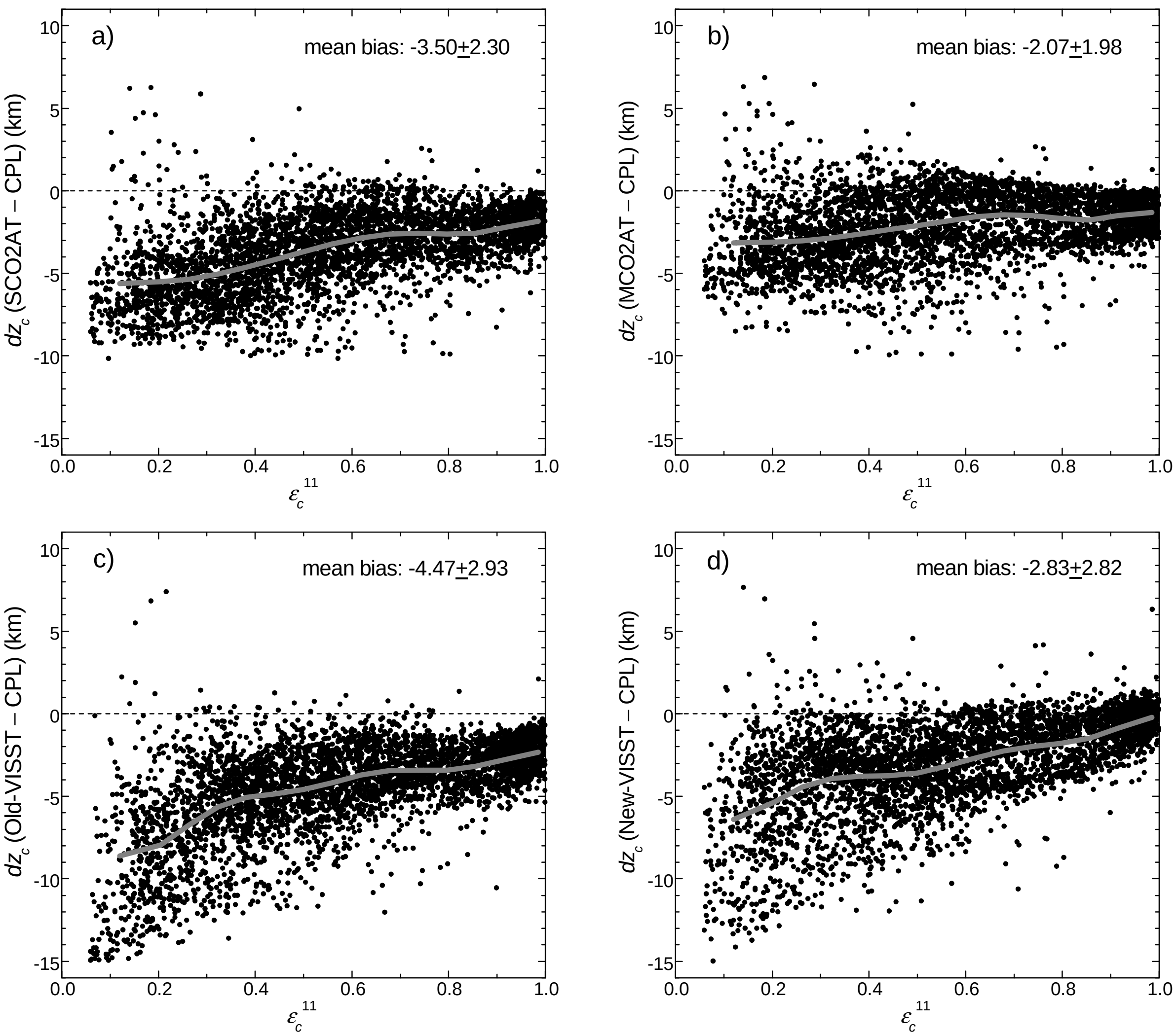

Fig. 5 CTH difference dz_c as a function of the 10.8-μm cloud effective emissivity ε_c^{11}. (a) for SCO2AT minus CPL. (b) for MCO2AT minus CPL. (c) for old VISST minus CPL. (d) for new VISST minus CPL. Thick-grey lines represent the running means.

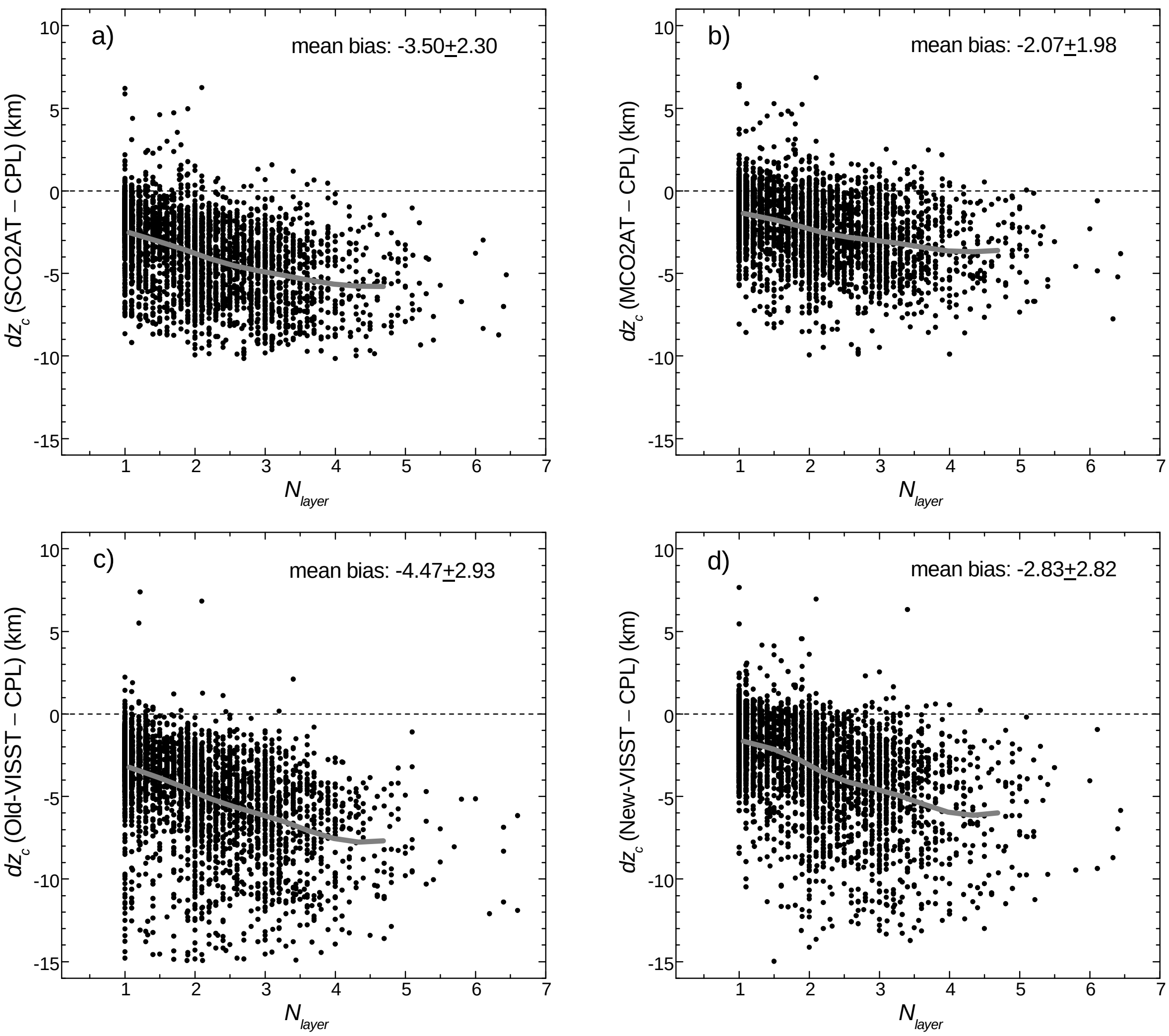

Fig. 6 CTH difference dz_c as a function of the number of cloud layers N_{layer}. (a) for SCO2AT minus CPL. (b) for MCO2AT minus CPL. (c) for old VISST minus CPL. (d) for new VISST minus CPL. Thick-grey lines represent the running means.

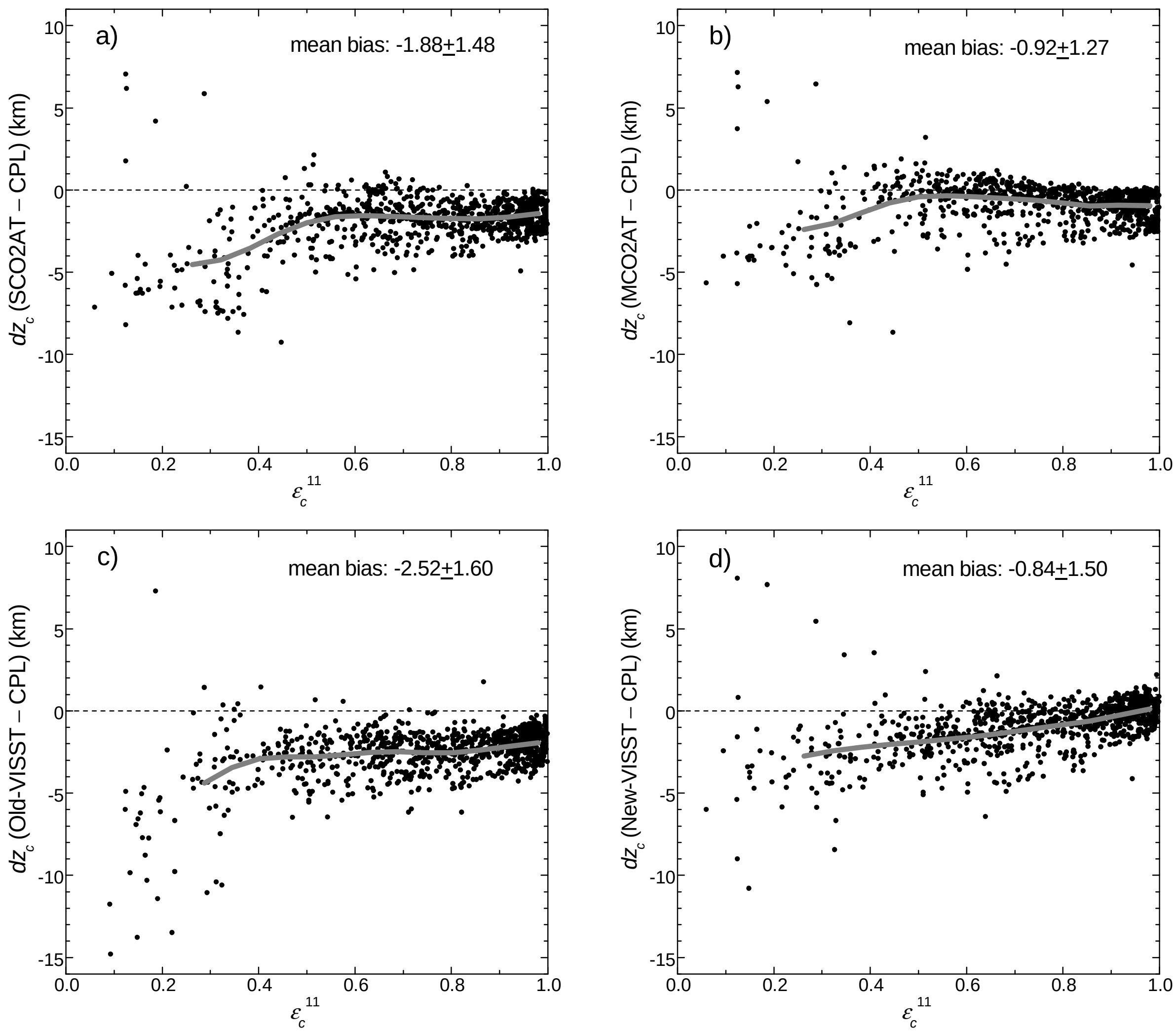

Fig. 7 Same as in Fig. 5, except for the single-layered (N_{layer} = 1) clouds.

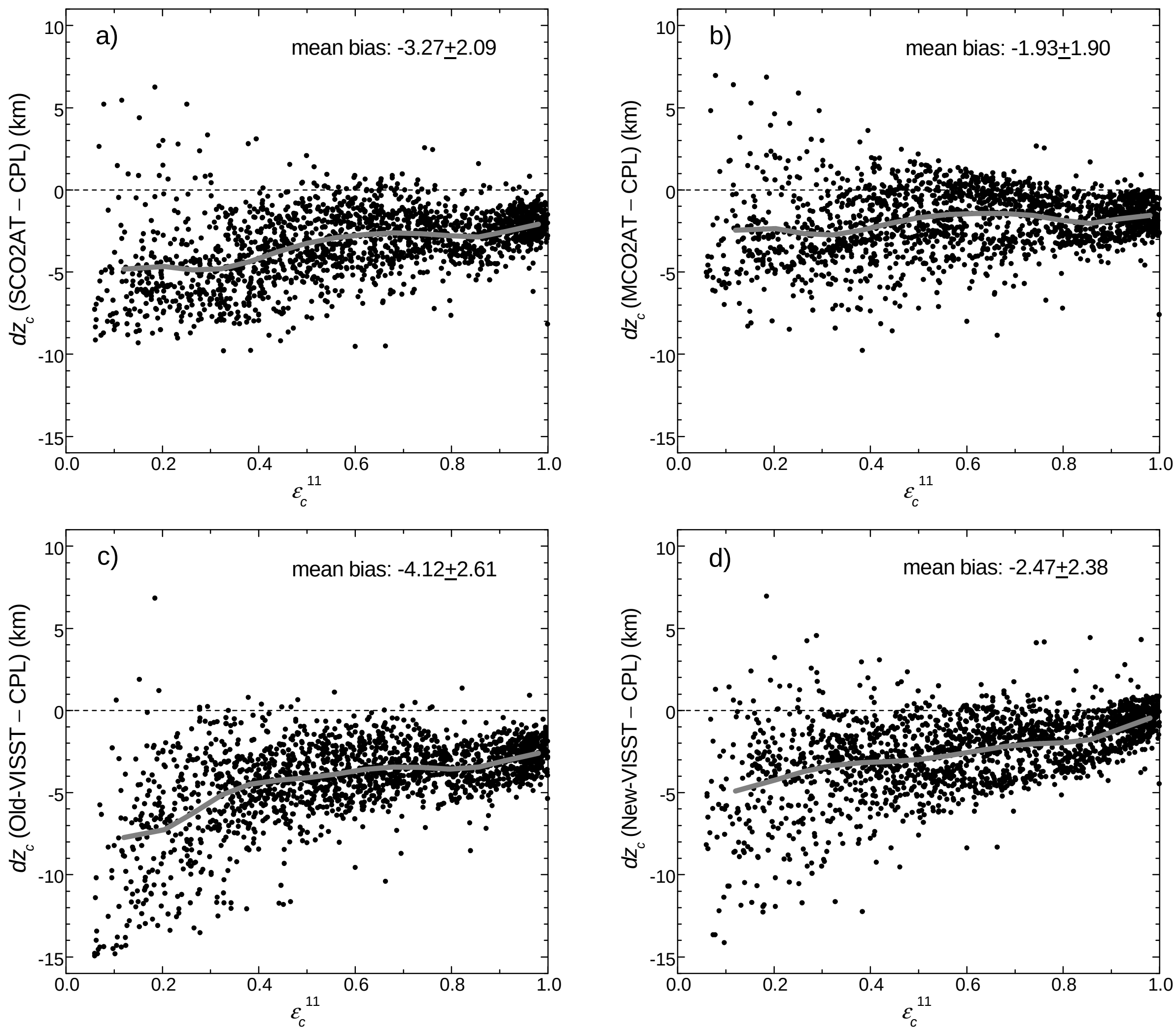

Fig. 8 Same as in Fig. 5, except for the two-layered ($1 < N_{layer} \leq 2$) clouds.

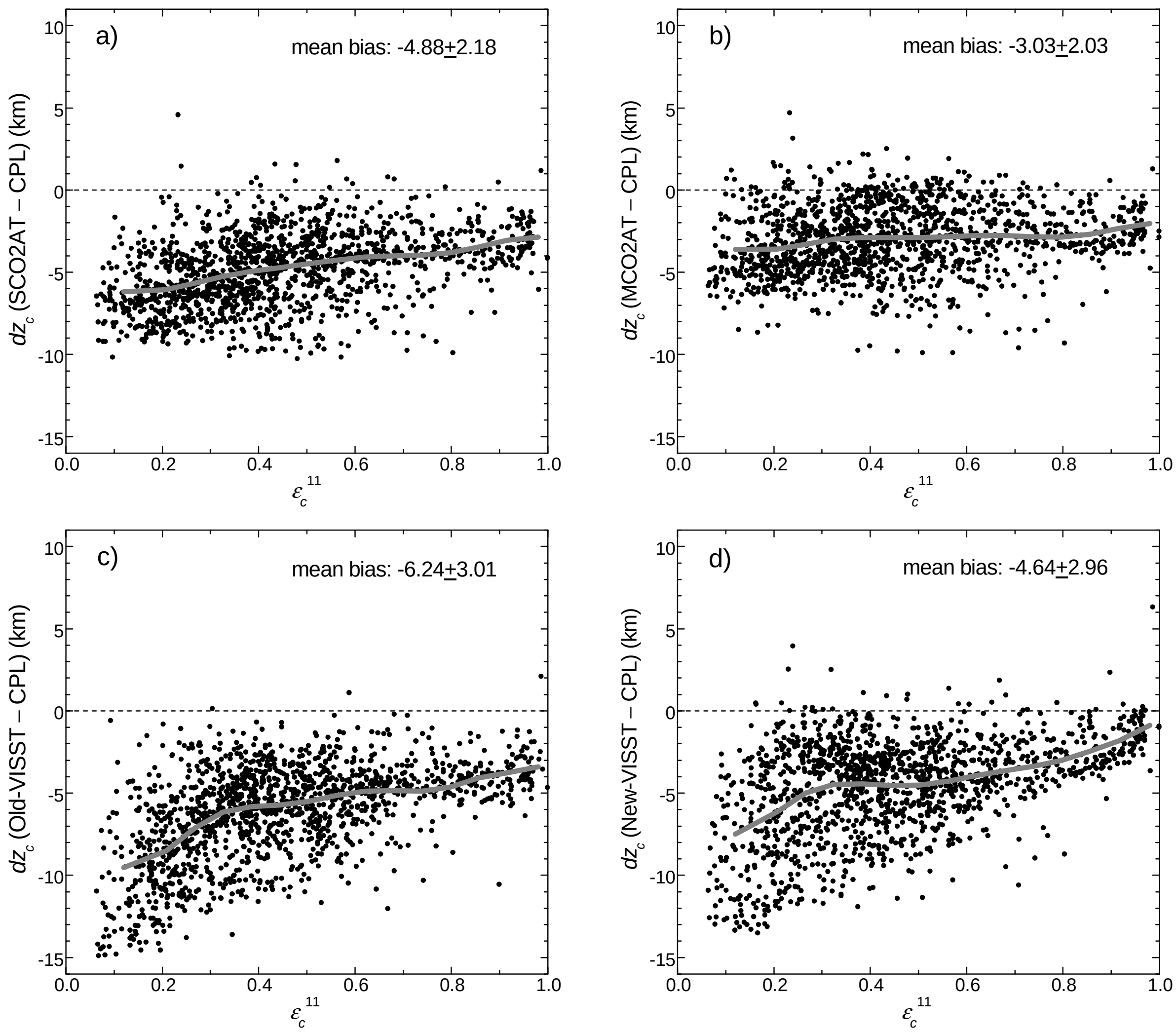

Fig. 9   Same as in Fig. 5, except for the multilayered ($N_{layer} > 2$) clouds.

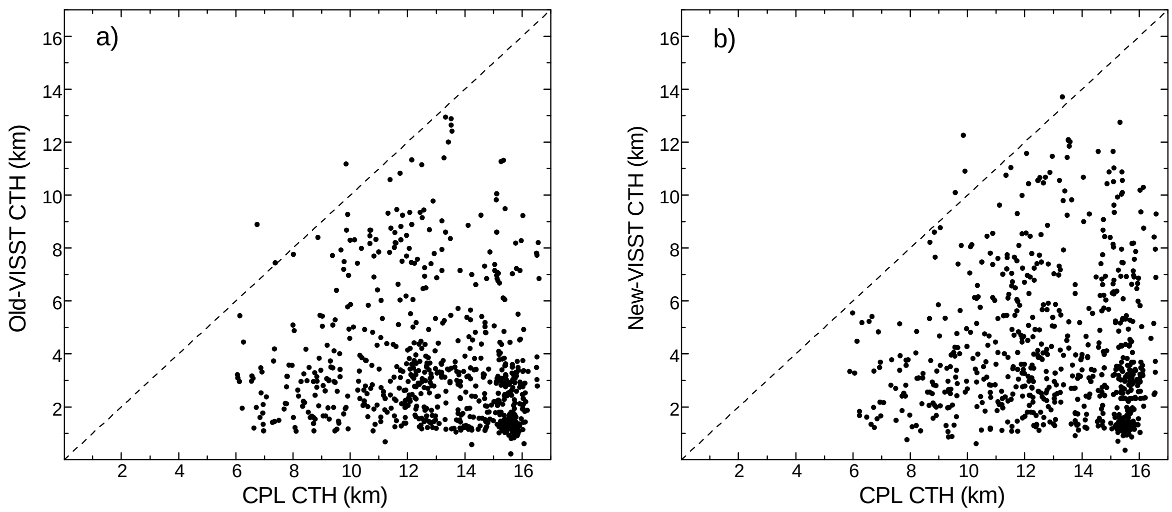

Fig. 10 Comparisons of the old-VISST (a) and new-VISST (b) CTHs with the CPL CTH when there was no SCO2AT/MCO2AT retrieval.